



Universidad Autónoma
de Madrid

Biblos-e Archivo
Repositorio Institucional UAM

Repositorio Institucional de la Universidad Autónoma de Madrid

<https://repositorio.uam.es>

Esta es la **versión de autor** del artículo publicado en:
This is an **author produced version** of a paper published in:

Journal of Chemical Theory and Computation 14.2 (2018): 820-832

DOI: <https://doi.org/10.1021/acs.jctc.7b01015>

Copyright: © 2017 American Chemical Society

El acceso a la versión del editor puede requerir la suscripción del recurso
Access to the published version may require subscription

A Mixed Quantum/Classical Method for Nonadiabatic Quantum Dynamics in Explicit Solvent Models: The $\pi\pi^*/n\pi^*$ Decay of Thymine in Water as a Test Case

Javier Cerezo,^{†,‡} Yanli Liu,^{¶,†} Na Lin,[§] Xian Zhao,[§] Roberto Improta,^{||,⊥} and
Fabrizio Santoro^{*,†}

[†]*CNR–Consiglio Nazionale delle Ricerche, Istituto di Chimica dei Composti Organo
Metallici (ICCOM-CNR), SS di Pisa, Area della Ricerca, via G. Moruzzi 1, I-56124 Pisa,
Italy*

[‡]*Departamento de Química Física, Universidad de Murcia, 30100 Murcia, Spain*

[¶]*School of Physics and Optoelectronics Engineering, Ludong University, 264025 Yantai, P.
R. China*

[§]*State Key Laboratory of Crystal Materials, Shandong University, 250100 Jinan, Shandong,
P. R. China*

^{||}*CNR–Consiglio Nazionale delle Ricerche, Istituto di Biostrutture e Bioimmagini
(IBB-CNR), via Mezzocannone 16, I-80136 Napoli, Italy*

[⊥]*LIDYL, CEA, CNRS, Université Paris-Saclay, F-91191 Gif-sur-Yvette, France*

E-mail: fabrizio.santoro@pi.iccom.cnr.it

Abstract

We present a novel mixed quantum classical dynamical method to include solvent effects on internal conversion (IC) processes. All the solute degrees of freedom are represented by a wavepacket moving according to nonadiabatic quantum dynamics, while the motion of an explicit solvent model is described by an ensemble of classical trajectories. The mutual coupling of the solute and solvent dynamics is included within a mean-field framework and the quantum and classical equations of motions are solved simultaneously. As a test case we apply our method to the ultrafast $\pi\pi^* \rightarrow n\pi^*$ decay of Thymine in water. Solvent dynamical response modifies IC yield already on the 50 fs timescale. This effect is due to water librational motions that stabilize the most populated state. Pure static disorder, i.e. the existence of different solvent configurations when photoexcitation takes place, also has a remarkable impact on the dynamics.

1 Introduction

Solvent can deeply affect internal conversions (IC) at Conical Intersections (CoIs),¹ especially when the coupled states are characterized by remarkably different charge densities and/or different networks of specific interactions with solvent molecules. Although in principle quantum dynamics (QD) is the most accurate framework to describe IC processes and notwithstanding the impressive potentialities of Multi-configurational Time-Dependent Hartree (MCTDH),²⁻⁷ a straightforward solution of the time-dependent (TD) Schrödinger equation (TDSE) for solute+solvent is, at the state of the art, not possible. Popular approximate QD methods describe solvent effects in terms of the coupling of the solute coordinates to a density of states, renouncing to a molecular description of the solvent.⁸⁻¹² This approach

describes dissipative effects but does not provide an easy way to inquire the relevance for the IC dynamics of specific solvent motions (like H-bonds) and, often, implicitly assumes that the solvent moves as a bath of harmonic oscillators. In this contribution we thus propose a novel mixed quantum classical (MQC) model, tailored for rigid systems, that retains a full QD description of solute dynamics -exploiting the MCTDH method- and accounts for solvent effects through an explicit molecular model moving according to classical dynamics, as it happens in trajectory-based methods.¹³⁻¹⁵ Our approach is computationally effective and can treat solute/solvent interactions at different levels of sophistication (from molecular mechanics (MM) to quantum mechanics (QM)). It allows to take into account the intrinsically anharmonic nature of solvent dynamics (e.g librational and/or re-orientational motions) and to identify those specific solvent modes, if any, that interfere with the IC process.

The basic idea of our method is to solve simultaneously the QD Equations of Motion (EOMs) for the solute degrees of freedom (DoF) and the classical EOMs for solvent DoF (described by a swarm of trajectories) accounting for their mutual coupling in an approximate way. This is done within a mean-field approach, assuming that the solvent dynamics is driven by the TD average electronic density of the solute arising from the nonadiabatic dynamics on the coupled electronic states. At the same time, the motion of the solvent molecules introduces a time dependence of some parameters of the model Potential Energy Surfaces (PESs) of the solute.

Within our approach it is straightforward to consider solvent effects on the dynamics with different degrees of approximation, each one corresponding to a limit physical model. As a first basic approximation, one can simply perform dynamical calculations as in the gas phase but using the 'average' PES computed

in solution.¹⁶ A more refined model, as that adopted in ref.,¹⁷ considers what in the following we refer as 'static disorder': when photoexcitation takes place different solute/solvent arrangements are probed, each one characterized by slight different PES's. Finally, it is possible to go beyond this 'static' description of solvent effect, and this is the main novelty of our approach. It accounts for the fact that after photoexcitation the solvent can actually move on the timescale of the IC process and its movement is coupled to the IC photodynamics and modify its yield. In this contribution we will analyze in detail the relative importance of these different factors, by using the ultrafast $\pi\pi^* \rightarrow n\pi^*$ decay of photoexcited thymine (Thy, see Figure 1) in water solution as a test application. This process constitutes a hot topic in the field of DNA photoactivated dynamics, as witnessed by several very recent experimental,¹⁸⁻²¹ and computational studies (see ref.²² for a review). It is well assessed that an ethylenic type CoI (Eth-)CoI, occurring at a strongly distorted molecular structure, is the main responsible of the direct sub-ps non-radiative decay of $\pi\pi^*$ to the ground state (GS). Experiments, as well as the few dynamical computational studies available,^{16,19,23} provide instead contrasting indications on the involvement of the $n\pi^*$ state in the photoactivated dynamics and on the timescale associated to its population and de-population.¹⁸⁻²¹ Our novel MQC scheme shows that the population transfer is fast (< 100 fs) but its extent is extremely dependent on the solute/solvent interaction model. More importantly, our results highlight that dynamical solvent effects, related to response of the librational motions of water molecules, are already operative in 50 fs and strongly modulate Thy photoexcited dynamics. The $\pi\pi^*/n\pi^*$ coupled dynamics in Thy was selected for its intrinsic interest and as a prototypical case of an IC between two quasi-degenerate states that are sensitive to solvent motion. In this way we can provide general insights on the underlying chemical physical effects ruling ultrafast

nonadiabatic processes in solution.

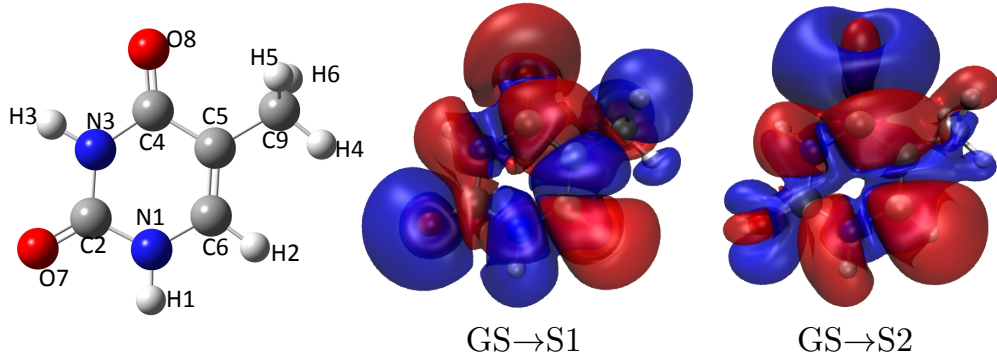


Figure 1: Structure of thymine with the number labels used in this work (left). Middle and right figures represent the difference density ($\Delta\rho = \rho^\gamma - \rho^{GS}$; where $\gamma = \pi\pi^*, n\pi^*$) corresponding to the transitions from GS to $\pi\pi^*$ (S1) and $n\pi^*$ (S2) states as isodensity surfaces at values $+2.5 \times 10^{-4}$ a.u. (red) and -2.5×10^{-4} a.u. (blue). PBE0/6-31+G(d,p) computations in water (PCM)

The method is presented in Section 2 and the computational details are given in Section 3. Section 4 reports the results which are further analyzed in Section 5 where we also provide a discussion on the limitations and possible developments of the method. Section 6 gives some concluding remarks.

2 The method

Let us consider the super-system composed by the solute (s) and the solvent (b), a suitable set of their coordinates, \mathbf{q}_s and \mathbf{Q}_B , that will be specified in the following, and the two solute diabatic states $|\pi\pi^*\rangle$ and $|n\pi^*\rangle$. We indicate the Hamiltonian of the super-system with the symbol \mathcal{H} ,

$$\mathcal{H} = \mathcal{H}_\pi(\mathbf{q}_s, \mathbf{Q}_B, \mathbf{p}_s, \mathbf{P}_B)|\pi\pi^*\rangle\langle\pi\pi^*| + \mathcal{H}_n(\mathbf{q}_s, \mathbf{Q}_B, \mathbf{p}_s, \mathbf{P}_B)|n\pi^*\rangle\langle n\pi^*| + \mathcal{V}_{n\pi}(\mathbf{q}_s, \mathbf{Q}_B)(|n\pi^*\rangle\langle\pi\pi^*| + h.c.) \quad (1)$$

where h.c. stands for hermitian conjugate. The core of our protocol is to treat the coordinates \mathbf{Q}_B and the associated momenta \mathbf{P}_B as classical TD parameters, and not as quantum operators. Therefore the wavefunction of the system $|\Psi(t)\rangle$ depends only on the quantum DoFs \mathbf{q}_s (and this will be specified by a “s” superscript on the wavefunction) and its time evolution is ruled by a TD Hamiltonian,

$$i\hbar\partial_t\Psi^s(\mathbf{q}_s, t) = \mathcal{H}(\mathbf{Q}_B(t), \mathbf{P}_B(t))\Psi^s(\mathbf{q}_s, t) . \quad (2)$$

On the other hand, the quantities $(\mathbf{Q}_B, \mathbf{P}_B)$ evolve as classical variables, subject to forces that are represented by the mean TD Hamiltonian

$$\langle\mathcal{H}\rangle(\mathbf{Q}_B, \mathbf{P}_B, t) = \frac{\langle\Psi^s(t)|\mathcal{H}(\mathbf{Q}_B, \mathbf{P}_B)|\Psi^s(t)\rangle}{\langle\Psi^s(t)|\Psi^s(t)\rangle} , \quad (3)$$

For a Hamiltonian evolution they are

$$\dot{\mathbf{Q}}_B = \frac{\partial\langle\mathcal{H}\rangle}{\partial\mathbf{P}_B} ; \quad (4a)$$

$$\dot{\mathbf{P}}_B = -\frac{\partial\langle\mathcal{H}\rangle}{\partial\mathbf{Q}_B} . \quad (4b)$$

In summary, the simultaneous evolution of the quantum and classical DoFs is described by Eqs. (3) and (4a)-(4b), implying that the classical variables follow the mean field of the quantum part of the super-system. At the same time at time zero many different solvent configurations are possible and therefore the results of the dynamics must be averaged over a sufficient number of trajectories of the

classical DoFs.

To proceed further we now specify that \mathbf{Q}_B are the atomic Cartesian coordinates of the solvent molecules (and may comprise also the three translations and three rotations of the solute) and rewrite the Hamiltonian felt by the system as adopting ground-state normal coordinates \mathbf{q}_s

$$\begin{aligned}\mathcal{H}^s(t) &= \mathcal{H}_\pi^s(\mathbf{q}_s, \mathbf{Q}_B(t))|\pi\pi^*\rangle\langle\pi\pi^*| + \mathcal{H}_n^s(\mathbf{q}_s, \mathbf{Q}_B(t))|\text{n}\pi^*\rangle\langle\text{n}\pi^*| + \\ &\quad \mathcal{V}_{\text{n}\pi}^s(\mathbf{q}_s, \mathbf{Q}_B(t))(|\text{n}\pi^*\rangle\langle\pi\pi^*| + h.c.)\end{aligned}\quad (5)$$

$$\mathcal{H}_\gamma^s(\mathbf{q}_s, t) = \mathcal{T}^s + E_\gamma^0(t) + \boldsymbol{\lambda}_\gamma^T(t)\mathbf{q}_s + \mathbf{q}_s^T\mathbf{F}_\gamma(t)\mathbf{q}_s \quad (6)$$

$$\mathcal{V}_{\text{n}\pi}^s(\mathbf{q}_s, t) = V_{\text{n}\pi}^0(t) + \boldsymbol{\lambda}_{\text{n}\pi}^T(t)\mathbf{q}_s + \mathbf{q}_s^T\mathbf{F}_{\text{n}\pi}(t)\mathbf{q}_s \quad (7)$$

where $\gamma = \pi, n$ and \mathcal{T}^s is the kinetic operator of the solute DoFs. Eqs. 6-7 defines what is usually known as Quadratic Vibronic Coupling (QVC) model.²⁴ It rules the evolution of the solute wavefunction, $|\Psi^s(t)\rangle = |\pi\pi^*\rangle\psi_\pi(\mathbf{q}_s, t) + |\text{n}\pi^*\rangle\psi_n(\mathbf{q}_s, t)$, where the nuclear wavepackets $\psi_\pi(\mathbf{q}_s, t)$ and $\psi_n(\mathbf{q}_s, t)$ depend on all the solute normal coordinates and on time. In principle, all the potential terms in Eqs. 6-7 depend on time through the classical variables $\mathbf{Q}_B(t)$ and indirectly account also for the couplings of \mathbf{q}_s and \mathbf{Q}_B coordinates.

In this first implementation of the method the classical dynamics of the solvent is ruled by a standard Molecular-Mechanics (MM) Force Field (FF). The FF accounts for intra- and intermolecular interactions involving solvent molecules by standard potential terms generally indicated in the following as \mathcal{V}^{BB} . The interaction between the solute and the solvent is described by a sum of Lennard Jones (LJ) and Coulomb terms, $\mathcal{V}_{LJ}^{sB}(t)$ and $\mathcal{V}_{el}^{sB}(t)$, whose time-dependence arises from the propagation of solute vibronic wavefunction. The computation of the average

in Eqs.4a-4b involves both $\mathcal{V}_{LJ}^{sB}(t)$ and $\mathcal{V}_{el}^{sB}(t)$ and in practice it is approximated by introducing the average values at time t of the solute atomic positions and atomic charges $\zeta=(\zeta_1, \zeta_2, \cdot \cdot, \zeta_N)$ where N is the number of nuclei of the solute.

$$\mathcal{H}^B(\mathbf{Q}_B, \langle \mathbf{q}_s \rangle(t), \langle \zeta \rangle(t)) = \mathcal{H}^B + V^{sB}(t) = \mathcal{T}^B + \mathcal{V}^{BB} + \mathcal{V}_{LJ}^{sB}(\langle \mathbf{q}_s \rangle(t)) + \mathcal{V}_{el}^{sB}(\langle \mathbf{q}_s \rangle(t), \langle \zeta \rangle(t)) \quad (8)$$

Notice that according to the adopted mean-field approximation (Eqs.4a and 4b) the solvent moves in a average potential due to the solute. In other words, the solvent does not feel two different potentials for the solute in $|\pi\pi^*\rangle$ and $|\text{n}\pi^*\rangle$, but a potential averaged on both the electronic states. Since $|\Psi(t) = |\pi\pi^*\rangle|\psi_\pi(t)\rangle + |\text{n}\pi^*\rangle|\psi_n(t)\rangle$, for the partial charge assigned to a specific nucleus j and for a specific normal coordinate $(q_s)_i$ we have

$$\langle \zeta_j \rangle(t) = |\langle \psi_\pi(t) | \psi_\pi(t) \rangle|^2 \zeta_j^\pi + |\langle \psi_n(t) | \psi_n(t) \rangle|^2 \zeta_j^n \quad (9)$$

$$\langle (q_s)_i \rangle(t) = \langle \psi_\pi(t) | (q_s)_i | \psi_\pi(t) \rangle + \langle \psi_n(t) | (q_s)_i | \psi_n(t) \rangle \quad (10)$$

In Eq.9 the average atomic charges is obtained from the atomic charges of the $\pi\pi^*$ (ζ^π) and $\text{n}\pi^*$ (ζ^n) states weighted for the electronic populations $P_\pi = |\langle \psi_\pi(t) | \psi_\pi(t) \rangle|^2$ and $P_n = |\langle \psi_n(t) | \psi_n(t) \rangle|^2$ (with $P_\pi = 1 - P_n$). Similarly, the expectation values of the normal coordinates treated at quantum level (Eq.10) are a weighted average on the two electronic states.

The theoretical framework presented above is rather general. One might consider harmonic approximation of the solute diabatic PES in Eqs. 6-7 simply as a “local expansion” of the potentials. Updating the Hessian and gradients at each

step during the (solute+solvent) dynamics it would be possible to run a coupled QD-MD simulation fully on-the-fly, i.e. without adopting predetermined PESs, for example describing the wavepacket in terms of localized Gaussians,^{25,26} and adopting the so-called Direct Dynamics-variational Multiconfigurational Gaussian (DD-vMCG) method.^{27,28} This would allow to account not only for solute-solvent interactions but also for any anharmonicity of the solute PES. Due to its computational cost, the application of DD-vMCG is currently mostly confined to small molecules in gas phase.^{29,30}

2.1 A simplified model: focussing on the $\pi\pi^*/n\pi^*$ energy gap

Here we look for a simplified and necessarily approximate method that is amenable for an efficient implementation but still able to provide interesting insight into the dynamical solvent effects on the solute nonadiabatic dynamics. To that end, we now limit our analysis to rigid systems for which harmonic PES generally provide a reasonable description of the PES (this was actually implicit in the use of normal coordinates in Eqs.6-7). Second, we focus on the dynamical solvent effect on some of the parameters of the system Hamiltonian only. More specifically, we assume that the solvent fluctuations induce a rigid translation of the $\pi\pi^*$ and $n\pi^*$ PESs on the energy axis without altering their shape. This is clearly an approximation. However, the energy gap ($\Delta E_{n\pi}^0 = E_n^0 - E_\pi^0$) at the FC geometry is indeed a key parameter for the probability of a ultrafast population transfer. Actually, for the specific case we have studied, i.e. $\pi\pi^*/n\pi^*$ process of Thy, solvent can change $\Delta E_{n\pi}^0 = E_n^0 - E_\pi^0$ by 0.3-0.6 eV (depending on the solvent model) and it is the main factor determining the dynamics. We show in the following that different $\Delta E_{n\pi}^0$ produce different IC yields, while on the contrary (see SI) Hamiltonians

computed either in gas-phase or in water (with the polarizable continuum model, PCM)³¹ provide practically the same results if we constrain $\Delta E_{n\pi}^0(0)$ to have the same value.

Finally, we assume that the term independent of coordinates in the diabatic coupling, $V_{n\pi}^0(t)$ in Eq. 7, is vanishingly small (i.e. a true conical intersection exists). This means that in Eqs. 6 and 7 the only time-dependent parameters are the diagonal energy terms not depending on the coordinates (E_π^0 and E_n^0).

For the other parameters of the solute Hamiltonian we choose a mean-field approximation which is conveniently obtained by computing gradients ($\boldsymbol{\lambda}$) and Hessians (\mathbf{F}) in Eqs 6 and 7, accounting for average solvent effects with the polarizable continuum model (PCM).

As far as the solvent dynamics is concerned, consistently with the assumption that the solute moves in a mean-field PES (so that the instantaneous values of the solvent coordinates do not modify the forces felt by the solute coordinates), we also assume that the solvent motion is not altered by the small oscillations of the solute coordinates, and in the Force Field we substitute $\langle (q_s)_i \rangle(t) \approx (q_s(eq))_i$. In the mean-field framework this approximation is exact for the non-total (nt) symmetric coordinates $\langle (q_s^{nt})_i \rangle(t) = (q_s^{nt}(eq))_i = 0$.

2.2 Initial conditions

We now turn to the initial conditions of our problem. The solute must be represented by an initial wavepacket $|\Psi^s(0)\rangle$. As far as the solvent is concerned, many different configurations are possible at time $t=0$. The solvent phase space is explored by a preliminary MD around the solute considered in the ground state. From the resulting trajectory, a representative number of initial conditions ($\mathbf{Q}_B, \mathbf{P}_B$) are extracted.

In order to obtain such a mixed representation of the initial conditions a separation of the motions of s and B must be imposed, inasmuch to define a $|\Psi^s(0)\rangle$, and it necessary to establish a reference Hamiltonian of s in the GS that depends on \mathbf{q}_s coordinates only. In line with what done for the solute excited PESs, also the GS PES is obtained in harmonic approximation accounting for mean-field solvent effects with PCM; the initial $|\Psi_s(0)\rangle$ is the ground-vibrational state of the GS Hamiltonian, promoted on the bright state $\pi\pi^*$. Moreover, in line with the approximations described in the above section, the solvent GS distribution is explored with an MD (NVT ensemble) considering a rigid solute in its GS equilibrium position predicted by PCM (\mathbf{q}_s^{eq}), and a number N_J of uncorrelated snapshots are taken as initial conditions of the photoexcited dynamics. This is the procedure recently adopted with success to estimate the solvent inhomogeneous linewidth that broadens the quantum vibronic spectra in polar solvents.^{32,33}

3 Computational details

3.1 Electronic calculations and diabaticization

Electronic structure calculations were carried out with Density Functional Theory (DFT) and its time-dependent (TD) extension (TD-DFT) for excited states, as implemented in Gaussian09,³⁴ adopting PBE0 functional in combination with the 6-31+G(d,p) basis set. Model PES were computed accounting for mean solvent effects with PCM. More specifically the harmonic PES of the ground state was computed in C_s symmetry, determining its optimized geometry and normal modes and frequencies. As far as excited states (ES) are considered we focused on the two lowest adiabatic states S_1 and S_2 , which arise from the mixing of the two diabatic states $\pi\pi^*$ and $n\pi^*$ states. We performed TD-DFT calculations on S_1 and S_2 ,

describing solvent effects with the linear response (LR) implementation of PCM in the nonequilibrium regime.³¹ This is the most suitable choice to study ultrafast processes, in as much it assumes that only the fast polarization for the solvent equilibrates with the ES. The model PES for $\pi\pi^*$ and $n\pi^*$ states were defined taking as a reference the states at the C_s GS equilibrium geometry, where diabatic and adiabatic states coincide. In Eqs. 6 and 7 we introduced the general QVC model. In this first application of our QD-MD method we use the simpler and very popular Linear Vibronic Coupling (LVC) model, that can be derived from the QVC one by taking $\mathbf{F}_{n\pi} = 0$ and $\mathbf{F}_\pi = \mathbf{F}_n = \mathbf{\Lambda}_{GS}$ (with $\mathbf{\Lambda}_{GS}$ the diagonal force constant matrix in the GS).

We displaced the structure along each normal mode by $\pm\delta$ (6N-12 calculations) and then computed the diabatic states implementing the method proposed by Cimiraglia et al.³⁵ for Configuration-Interaction wave functions and by Neugebauer et al.³⁶ for TD-DFT. In practice for each displacement δ along mode i , the adiabatic states are combined so to obtain diabatic states that resemble as much as possible the reference states. This procedure allows to obtain, diabatic energies and couplings and therefore to compute the gradients of the diagonal PES ($\boldsymbol{\lambda}_\pi^s$ and $\boldsymbol{\lambda}_n^s$) and of the coupling ($\boldsymbol{\lambda}_{n\pi}^s$) by numerical differentiation. We set $\delta=0.1$ in dimensionless coordinates and checked that analogous results are obtained also increasing it to 0.2 and that the gradients of the diagonal PES (only non-vanishing along total symmetric coordinates) are very similar to those computed analytically by Gaussian09 for adiabatic states.

3.1.1 Computation of the vertical energies with explicit models

The excitation energies for the solute surrounded by explicit water molecules (including a sphere of 60 Å) was computed with a QM/MM strategy, including Thy

in the QM part (TDDFT). Two schemes PCsol and QMsol are used to describe the solvent. In the first one, all solvent molecules are treated as point charges using the partial charges from the TIP3P model (PCsol model). In the second one, water molecules at a distance of 5 Å from the center of Thy or at 2.3 Å from its oxygen and nitrogen atoms, so as solute-solvent hydrogen bonds are included, are treated at the QM level, while the rest are treated as point charges (QMsol model). In this case we checked that no spurious charge-transfer³⁷ occurs between Thy and the water molecules.

3.2 Quantum dynamics

QD calculations including all the 39 DoF of Thy were run with (ML)-MCTDH⁴⁻⁷ method implemented in Quantics code.³⁸ As a primitive basis set we adopted an Hermite DVR representation. Equations of motions were integrated following the examples provided for the 24D nonadiabatic dynamics of pyrazine, i.e. using a variable mean field (VMF) using Runge-Kutta integrator of order 5 and accuracy 10^{-7} . To check convergence we tested different numbers of SPFs and different dimensions of the primitive grids. The corresponding ML trees are reported in Figures S3 and S4 in the SI. The convergence of the electronic populations with the two ML expansion is shown in Figure S5 in the SI

3.3 Classical molecular dynamics in the ground state

MD simulations were performed imposing periodic boundary conditions (PBC) with a unit cell of $(66 \times 66 \times 66) \text{ Å}^3$, consisting of one Thy molecule and ~ 9300 water, treated with the TIP3P model. Solvent configuration was taken from an equilibrated system with density of 1 g/l so as to ensure a realistic solvent environment around the solute. The internal structure of Thy was restrained to be

close to the equilibrium geometry by imposing stiff harmonic potential over all internal coordinates. To account for the intermolecular interactions between Thy and water molecules a truncated Lennard-Jones (LJ) potential ($r_{cut-off} = 11 \text{ \AA}$) and a Coulomb potential treated with PME method were used. For Thy, LJ parameters were taken from AMBER03, while partial charges were derived using 2 different schemes: RESP³⁹ and CM5.⁴⁰

MD calculations were performed on a NVT ensemble at 300 K. The system is first equilibrated for 200 ps using the Berendsen thermostat ($\tau_T = 0.1 \text{ ps}$), which is then replaced by the Nosé-Hoover algorithm in the production step. A total time of 6 ns were simulated, applying constraints to all bonds involving hydrogen atoms and using a time step of 0.5 fs. The first 500 ps of the production step were discarded to ensure a proper equilibration with the updated thermostat.

Configurations were extracted along the MD simulations on the GS every 30 ps. Since the restraint potentials still allow small perturbations of the internal structure of Thymine, the structure at each snapshot was replaced by the equilibrium one, which is placed in a position where the root mean square deviation deviations with respect to the restrained geometry is minimal. Moreover, the velocities on the restrained structure are re-projected over to the equilibrium structure, using the Eckart frame as intermediate point and, in this process, the velocities associated to vibrational DoFs are set to zero. See SI for further details.

3.4 Mixed Quantum Classical (QD-MD) Excited State simulation

Solute quantum EOMs (ML-MCTDH) and solvent classical (Newton’s) EOMs must be solved simultaneously. This is done with in-house developed scripts that interface Quantics, Gromacs and Gaussian09. The Hamiltonians of each subset

(the solute and the solvent) are updated to include the effect of the time evolution of the other subset each Δt . The value of Δt is set to 5 fs which, according to our preliminary tests (shown in the SI), provides a good balance between accuracy and computational efficiency.

The time propagation is repeated for a representative number of initial configurations (and velocities) of the solvent extracted from the GS solvent MD, and the final results for the electronic populations are averaged over the trajectories. Each trajectory has an independent time-evolution and the computation can be trivially parallelized. This makes our QD-MD method an approximate but very efficient protocol to run nonadiabatic dynamics under the effect of explicit solvents.

The initial conditions (position and momenta) for all molecules in the system are taken from the snapshots extracted along the GS dynamics, after processing the structure of Thy as described above. The simulation is carried out imposing the same stiff harmonic potentials over all internal coordinates of Thy, restraining the equilibrium geometry. In order to ensure that Thy behaves as a rigid body in the MD part of the QD-MD simulation, the restrained structure is replaced by the equilibrium one every 1 fs and the velocities were re-projected, canceling the components over vibrational DoFs, as described above. Before cancellation, the velocities developed along vibrational DoFs correspond to a temperature below 17 K.

The same LJ parameters from the GS were adopted for all molecules in the system, while partial charges for Thy were updated during the dynamics according to Eq. 9. The simulation was conducted adopting an NVT ensemble but we checked that at the femtosecond timescale, the thermostat has no effect on the dynamics using a time step of 0.5 fs.

3.4.1 The algorithm of the QD-MD method

The algorithm of our method is presented as a flow chart in Figure 2

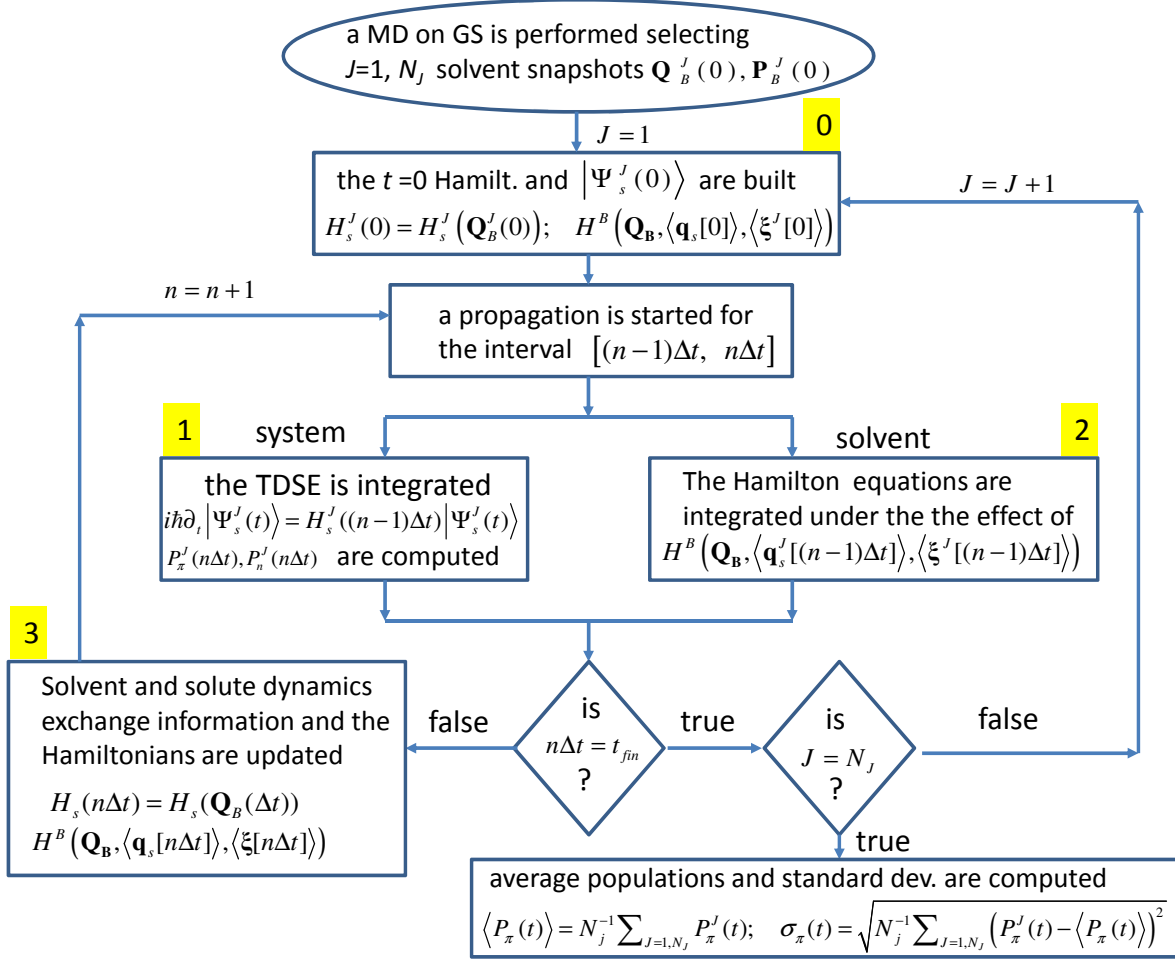


Figure 2: The flowchart of the method.

- For each solvent trajectory J , the QD-MD dynamical simulation is performed dividing the time interval from $t = 0$ to the final time t_{fin} in small steps Δt . Starting at $t = 0$ the initial wavepacket is promoted on the bright state $\pi\pi^*$ and propagated for Δt under the influence of $\mathcal{H}^s(0)$. At the same time the classical trajectory describing the solvent is propagated under the influence

of the Hamiltonian $\mathcal{H}^b(0)$ which depends on $\langle \mathbf{q}_s(0) \rangle = \mathbf{q}_s^{eq}$ and ζ_π . At each $t = n\Delta t$, \mathcal{H}^s and \mathcal{H}^b are updated. In these ways new steps of propagation are performed till the final time t_{fin} . The time-evolution is repeated for a representative number of initial configurations (and velocities) of the solvent and the final results are averaged over the N_J trajectories.

- at step (1) we solve the time dependent Schrödinger equation (TDSE) for a wavepacket depending on the solute 39 DoFs and moving on the coupled $\pi\pi^*$ and $n\pi^*$ PESs with ML-MCTDH approach.
- at step (2) the equations of motion of the solvent are solved for a solute frozen at $\langle \mathbf{q}_s((n-1)\Delta t) \rangle \approx \mathbf{q}_s^{eq}$ and charges $\langle \zeta^J((n-1)\Delta t) \rangle = P_n((n-1)\Delta t)\zeta_n + P_\pi((n-1)\Delta t)\zeta_\pi$, using Gromacs in a NVT ensemble (we checked that on this timescale NVE results are indistinguishable).
- at step (3) the solvent Hamiltonian $\mathcal{H}^b(\mathbf{Q}_B, \langle \zeta(n\Delta t) \rangle)$ is computed updating the solute charges. The solute Hamiltonian $\mathcal{H}_s^J(\mathbf{q}_s, t)$ is updated computing at TD-DFT/MM level the vertical energies of the two states $E_\pi^{0J}(n\Delta t)$ and $E_n^{0J}(n\Delta t)$ in the J snapshot of the solvent at time $t = n\Delta t$.

3.4.2 Simpler models for static solvent effects

Beyond the QD-MD scheme, we have also explored simpler models where the solvent effect is only static. In Av ΔE we investigate the *average* solvent effects on the energy gap by running a single dynamics with $\Delta E_{n\pi}^0(0)$ set to the value averaged over the solvent snapshots (or the single value obtained with PCM or in gas-phase). With Fluct ΔE we investigate the solvent static disorder, i.e. we account for the fact that each different solvent configuration at $t=0$ corresponds to a different energy gap, but we assume that the solvent is so slow to remain frozen

during the photodynamics. To this aim we run a different QD dynamics for each different $\Delta E_{n\pi}^0(0)$ (which does not change with time) corresponding to the selected snapshots and then average the results. The same “frozen-solvent” assumption was adopted by Thallmair et al.¹⁷ for QD photodissociations in condensed phase. Due to the nature of the problem, however, the authors did not use a Taylor expansion of the PES and computed them directly on a grid for a reduced dimensionality model (two internal coordinates), and they worked out a sophisticated method to include the effect of the specific snapshot of the solvent (extracted from a preliminary MD) at each point of the grid.

A schematic description of all the computational protocols adopted in this work is given in Table 1.

Table 1: Schematic description of the different computational protocols adopted in this work.

Thy charges for classical MD		QM/MM for excitation energies ^a
RESP		PCsol: solvent molecules as point charges
CM5		QMsol: first solvent shell QM, others point charges
Nonadiabatic dynamical simulations		
Model	Solvent Effect	Description
Av ΔE	Static, average	Energy gap from PCM, or from QMMM averaged over different solvent snapshots. P_π from a single QD dynamics with the average gap.
Fluct ΔE	Static disorder	A different QD dynamics for each energy gap corresponding to a different solvent snapshot. Gaps do not change with time. P_π averaged over all runs.
QD-MD	Dynamical	A different dynamics for each solvent snapshot. The solvent moves and QD (solute) and MD (solvent) are coupled. P_π averaged over all runs.

^a Thymine always in the QM region.

4 Results

The $\pi\pi^*$ and $n\pi^*$ states considered in this work are respectively the lowest bright and (almost) dark states of Thy (Figure S1 of SI) in the Franck-Condon (FC)

region, and are very close in energy. They correspond to a HOMO→LUMO and HOMO-1→LUMO transition, respectively (Molecular Orbitals, MOs, shown in Figure S2 of SI).

4.1 Average static solvent effect

Table 2 reports the vertical excitation energies of $\pi\pi^*$ and $n\pi^*$ computed at the GS minimum by TD-PBE0/6-31+G(d,p) in the gas phase and in water by using six different protocols to include solvent effects. Two of them adopt PCM (LR-PCM or State-Specific(SS)-PCM),⁴¹ and the other ones use explicit solvent models. In these cases we report the average value and the standard deviation over a set of 200 solvent configurations. Noteworthy the standard deviations here reported are directly related to the solvent inhomogeneous broadening of the transition.³²

In gas-phase predicted vertical energies are very similar to those computed with CR-EOM-CCSD(T)/aug-cc-pVTZ ($E_n^0=4.85$ and $E_\pi^0=5.15$ eV) and with MS-CASPT2/TZVP (4.94 and 5.06 eV).⁴²

In water $n\pi^*$ and $\pi\pi^*$ are strongly destabilized and slightly stabilized, respectively, with respect to gas phase,²² but the extent remarkably depends on the solvent model. The solvent blue-shift of $n\pi^*$ is in the range 0.25~0.45 eV, being larger for SS-PCM and RESP/QMsol models. It is caused by the depletion of the electron density on the Oxygen O8, (see Figure 1) which lead to a weakening of the H-bond with water molecules. The redshift of $\pi\pi^*$ is 0.02-0.13 eV and is larger when QM solvent molecules are included (QMsol). Solvent ensembles generated with RESP charges predict larger average solvent shifts and standard deviations because RESP charges are significantly bigger than CM5 ones (Table S2 in SI). The energy gap between the two states at the FC point, $\Delta E_{n\pi}^0$, thus critically depends on the choice of the solvation model. We checked that extension of the

basis set to 6-311+G(2d,2p) lead to very moderate changes on the energy gap: ~ 0.04 eV (see also ref.⁴³). On the balance $\Delta E_{n\pi}^0$ changes by $0.3\sim 0.6$ eV when going from the gas phase in water; the largest values are obtained when solvent molecules are included at the QM level. RI-CC2/aug-cc-pVDZ on a Thy+6H₂O cluster in combination with a COSMO implicit solvent model predicts $E_n^0=5.48$ and $E_\pi^0=5.08$ eV, i.e. $\Delta E_{n\pi}^0=0.4$ eV, with an increase of the energy gap from gas phase to water by 0.69 eV.⁴⁴

In the following we discuss the results obtained with all proposed protocols. The last part of the discussion will be however devoted to compare with experiment our best estimate for $\pi\pi^*/n\pi^*$ population transfer.

Table 2: Analysis of the average vertical excitation energies along the MD snapshots (standard deviations in parenthesis), and comparison with PCM values. All quantities in eV.

	PBE0						
	MD/CM5		MD/RESP		SS-PCM	LR-PCM	GP
	QMsol	PCsol	QMsol	PCsol			
E_π^0	5.004(0.071)	5.095(0.058)	5.017(0.067)	5.115(0.054)	5.075	5.056	5.130
E_n^0	5.141(0.112)	5.121(0.104)	5.296(0.125)	5.272(0.126)	5.289	5.095	4.870
$\Delta E_{n\pi}^0$	0.137(0.151)	0.027(0.135)	0.279(0.158)	0.157(0.155)	0.214	0.039	-0.260

Figure 3a reports the decay of the $\pi\pi^*$ population (P_π) in the gas phase and in water solution. In this latter case we always adopted the Hamiltonian parametrized with LR-PCM and we set $\Delta E_{n\pi}^0$ to the different average values given in Table 2 (Av ΔE model, Table 1).

The different values for $\Delta E_{n\pi}^0$ in Table 2 have a huge impact on the ultrafast $\pi\pi^*/n\pi^*$ dynamics. In gas phase, $\sim 90\%$ of the photoexcited population decays on $n\pi^*$ state ($P_n=1-P_\pi$) already within the first 100 fs. This finding is in very nice agreement with the decay time of 60 fs recently observed in ref.⁴⁵ and supports the reliability of our simulations. P_n is much smaller in water, and the amount

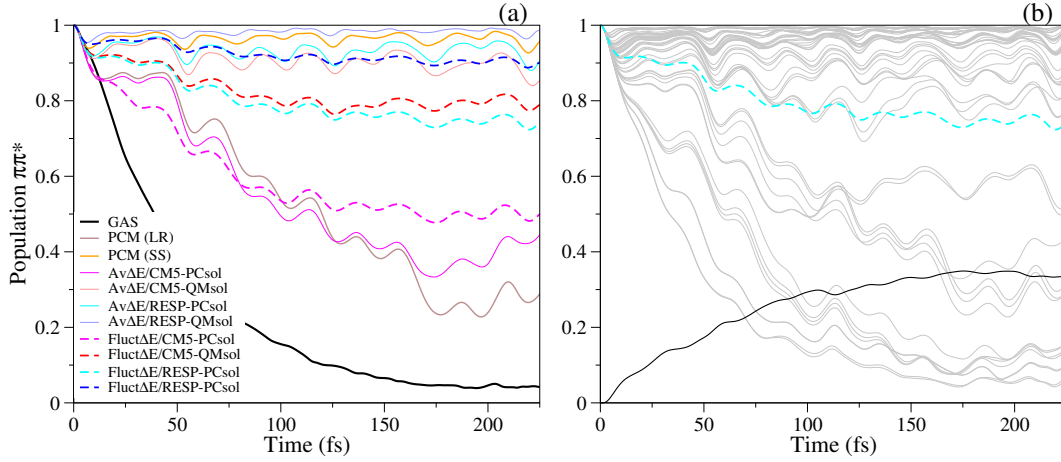


Figure 3: Decay of the P_π in gas-phase and in water solution, without accounting for solvent dynamical effects. Left: results on PESs with $\Delta E_{n\pi}$ obtained either at PCM level (LR or SS regimes) or computed from the average (Av ΔE) of the QM/MM energy gaps of 50 snapshots extracted from a MD run using CM5 or RESP solute charges. The average of the populations obtained with 50 different QD simulations, setting for each of them $\Delta E_{n\pi}$ to the value of the corresponding snapshot are also given as dashed lines (Fluct ΔE). In these cases the statistical uncertainty at the final time $t=230$ fs, due to the limited number of trajectories adopted is estimated to be 0.03, see next section. Right: Decay of P_π for all the 50 trajectories (gray) adopted to compute Fluct ΔE results with RESP/PCsol model. The average (cyan, the same given in left panel) and the standard deviation (dark gray) are also shown.

of population transferred to $n\pi^*$ strongly depends on $\Delta E_{n\pi}^0$, decreasing at the increase of $\Delta E_{n\pi}^0$. The long time limit of P_n ranges from ~ 0.7 (LR-PCM) to ~ 0.02 (Av ΔE /RESP/QMsol).

4.2 Effect of solvent static disorder. Fluct ΔE model

In order to account for static disorder we resorted to the Fluct ΔE model (Table 1). The results averaged over 50 trajectories (a subset of the initial 200 snapshots, according to the resampling strategy described in detail in the next section) are shown in Figure 3b for RESP/PCsol model. P_π evolution depends drastically on $\Delta E_{n\pi}^0$ values, with different trajectories showing transfers to $n\pi^*$ ranging from almost zero to 100%.

On the average, Fluct ΔE calculations predict a larger population transfer than

Av ΔE ones (continuous and dashed lines in Figure 3a), especially for cases where the transfer is weak. For example, according to RESP/PCsol model, after 230 fs Fluct ΔE predicts that P_n is almost three times as large ($\sim 22\%$ vs $\sim 8\%$). An intuitive explanation is provided by the different trajectories reported in Figure 3b. The amount of population transfer to $n\pi^*$ is not a linear function of $\Delta E_{n\pi}^0$. Solvent fluctuations that decrease $\Delta E_{n\pi}^0$ have a much larger impact on P_π (in some cases causing a 100% transfer) than those that further increase $\Delta E_{n\pi}^0$, and this causes a net increase of the average transfer. Shortly, in cases of weak (or strong) transfer, the effect of the wings of the solvent distribution can be very relevant and it is not adequately described by models that merely account for average effects (as Av ΔE).

4.3 Coupled QD-MD dynamics

The above results document that $\Delta E_{n\pi}^0$ plays a key role in determining the $\pi\pi^*/n\pi^*$. In the following we use our new QD-MD method to investigate how the effect of solvation dynamics on this parameter affects the IC rate. We start presenting test calculations to determine the number of trajectories necessary to achieve a reasonable convergence of the electronic populations.

4.3.1 Convergence of QD-MD results with respect to the number of trajectories

In Section 4.1, for each investigated solvent model we extracted a large number of snapshots (200) in the ground state to ensure a good convergence of the energy gap $\Delta E_{n\pi}^0$ and its standard deviation (Table 2). To speed up calculations, the coupled QD-MD simulations were run only for a subset of the possible snapshots. In order to estimate the accuracy of such procedure we selected one case, namely

RESP/PCsol, and we first computed the QD-MD considering all the 200 starting configurations (green line). From these trajectories, we then selected 20 sets of 25 or 50 trajectories. Two different types of sets were formed: either picking the trajectories randomly (“Random”) or ensuring that the resulting distribution of initial energy gaps has the same average and standard deviation as the one computed for the initial set of 200 configurations (“Resampling”). The results in Figure 4 indicate that the dispersion of the results with 25 trajectories is rather large. Moreover, even though the “Resampling” protocol reduces the variability over the initial femtoseconds with respect to the “Random” sets, the standard deviation at the end of the simulation is similar in both cases. When the number of trajectories is increased to 50, the differences between the results for “Random” and “Resampling” sets is noticeable even at the end of the simulation, and the variability is specially reduced in the case of the “Resampling” protocol, dropping from ~ 0.05 to ~ 0.03 . We therefore decided to adopt the “Resampling” protocol with 50 trajectories in the production runs of the paper. We note that the residual variability is smaller than the deviations associated to the different protocols applied in this work (e.g. Fluct ΔE vs. QD-MD; PCsol vs. QMsol or RESP vs. CM5).

A simpler and popular protocol to check the convergence, for example in TSH calculations, is to select a number of trajectories and then increase it and compare the results. For our QD-MD scheme, we tested this procedure selecting 25 trajectories and then increasing them to 50 and we found that it erroneously suggested that 25 results were perfectly converged (accuracy < 0.01) while they were not; the presence in the larger set of the first 25 trajectories, in fact, naturally increases the similarity of the predictions of the two calculations.

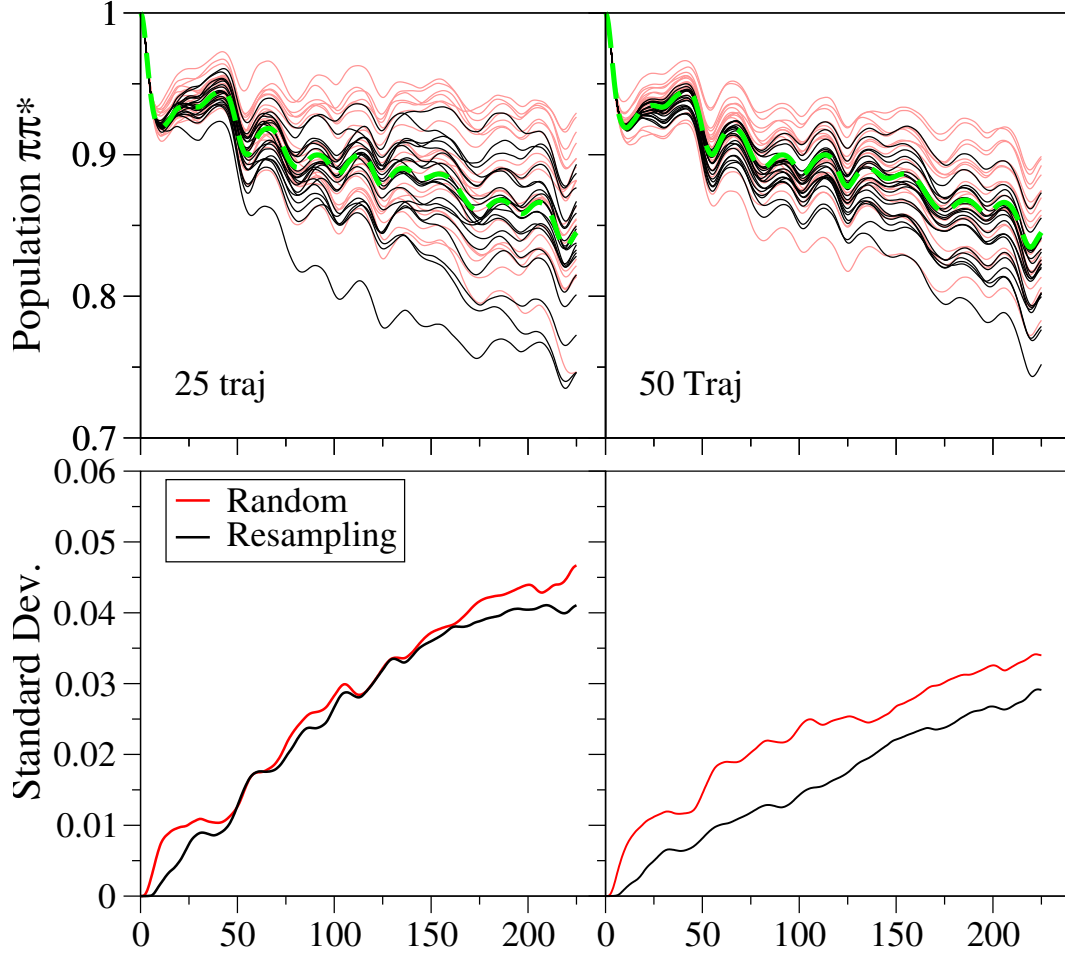


Figure 4: Population of the $\pi\pi^*$ corresponding to the averages over 25 or 50 trajectories with the RESP/PCsol model. In pale red, we show the results for 20 different sets picked randomly over a total of 200 snapshots, while in black we show 20 trajectories with sets that are generated so that the average and standard deviation is the same as the one computed with 200 snapshots. In green, we include the results for 100 trajectories. In the bottom panel, we show the standard deviation of the 20 different sets.

4.3.2 Dynamical solvent effect

To run our QD-MD scheme, we considered the same 50 representative snapshots of the GS solvent distribution selected in $\text{Fluct}\Delta E$ calculation (positions and velocities), for each of them we computed the time evolution of P_π , and then performed the average. Average populations with three different models for the solvent, RESP/QMsol, RESP/PCsol and CM5/PCsol, are shown in Figure 5a and compared with those that only include static disorder ($\text{Fluct}\Delta E$). Figure 5b shows the time evolution of P_π for all the trajectories computed with RESP/QMsol model.

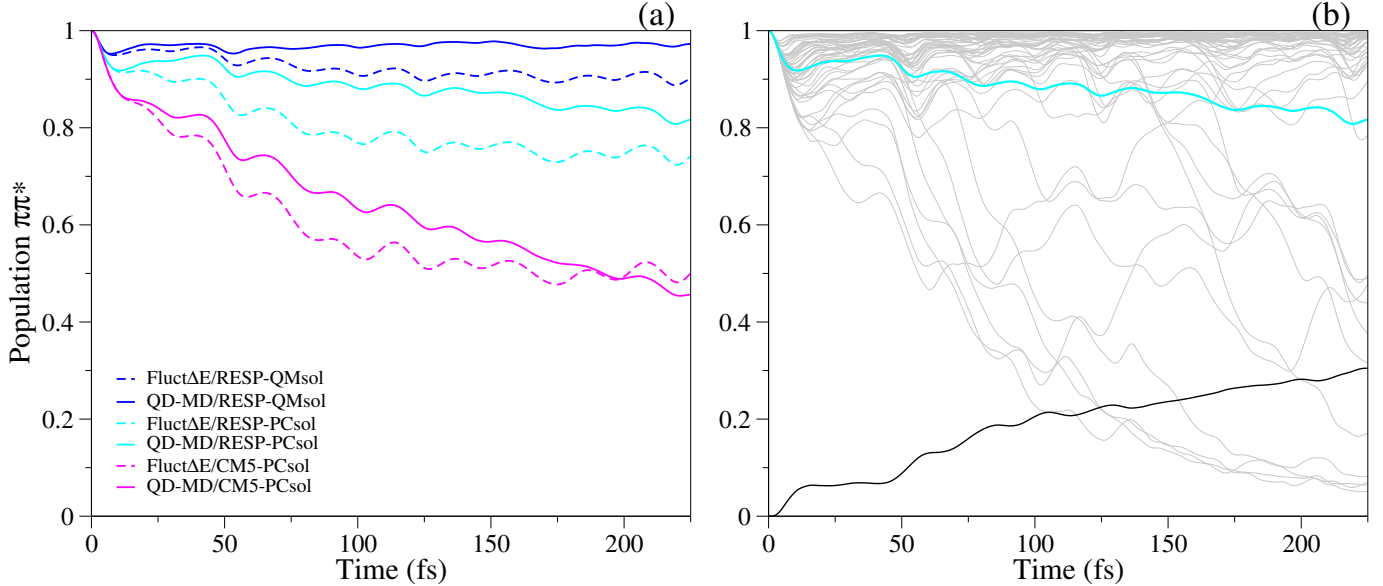


Figure 5: Left: Comparison of the P_π decay in water solution averaged over 50 solvent snapshots, accounting either for static ($\text{Fluct}\Delta E$) or for both static and dynamic solvent effects (MQC). Right: Decay of P_π corresponding to the 50 trajectories (gray) accounting for the dynamical solvent effects (MQC) with QMsol/RESP model. The average (blue) and the standard deviation (dark gray) are also shown. The statistical uncertainty on the average population at the final time $t=230$ fs, due to the limited number of trajectories adopted, is estimated to be ~ 0.03 .

The dynamics of solvent DoFs remarkably affects population transfer. Figure 5 actually shows that, already at times $t < 50$ fs, the QD-MD method predicts a P_π larger than for the $\text{Fluct}\Delta E$ case. On a longer time-scale, the decrease of population transfer to $n\pi^*$ due to solvent dynamics is larger when the intrinsic tendency

of the system to populate $n\pi^*$ is smaller, i.e. for RESP/QMsol model. This finding can be rationalized with the help of Figure 6, where the time evolution of the $\Delta E_{n\pi}^0$ during the coupled QD-MD, averaged over the 50 trajectories, is reported. For RESP/QMsol, $\Delta E_{n\pi}^0$ increases rapidly because the $\pi\pi^*$ state is largely more populated, solvent motions further stabilize it and makes the population transfer to $n\pi^*$ very unfavorable.

In other cases (RESP/PCsol and especially CM5/PCsol) $n\pi^*$ is more stable and therefore is populated more effectively. In such a situation, at times when both states are significantly populated, the solvent feels solute charges that are intermediate between $\pi\pi^*$ and $n\pi^*$ values (Eq. 9). Therefore the driving force to stabilize $\pi\pi^*$ vanishes, $\Delta E_{n\pi}^0$ may even start decreasing with time (Figure 6), and the difference between $\text{Fluct}\Delta E$ and QD-MD results becomes smaller or even changes sign (Figure 5).

To get further insight on the solvent effect, in Figure 6 we report three additional evolutions of $\Delta E_{n\pi}^0$ with RESP/PCsol model, averaged over the same 50 trajectories, assuming that the solute is frozen respectively in $\pi\pi^*$, in $n\pi^*$ or in GS. Due to the small population transfer to $n\pi^*$, the time evolution of $\Delta E_{n\pi}^0$ for the coupled $\pi\pi^*/n\pi^*$ case is quite similar to what seen when the solute is frozen in $\pi\pi^*$ state. Conversely, when the solute is frozen on $n\pi^*$ solvent dynamics has an opposite effect, leading to a progressive and remarkable decrease of $\Delta E_{n\pi}^0$. Finally, for a dynamics in GS, $\Delta E_{n\pi}^0$ remains approximatively constant with time. This evidence confirms that the variation of $\Delta E_{n\pi}^0$ is actually driven by the change of the solute density from GS to the specific photoexcited state. In addition to this general trend, $\Delta E_{n\pi}^0$ shows some fluctuations. Fast O-H stretching oscillations in water appear as small steps in the profiles in Figure 6. Decreasing the Δt from 5 to 1 fs provides smoother lines (see SI). Such improvement requires a significant

increase of the computational time but has shown in the previous section has a small effect on the populations. On top of this behavior, some weak oscillations with a period of ~ 50 -70 fs are observed both in the QD-MD coupled dynamics and for dynamics in $\pi\pi^*$, $n\pi^*$ or in GS. Their frequency, $\sim 650 - 470 \text{ cm}^{-1}$ lies in the region of the librational spectrum^{46,47} of water.

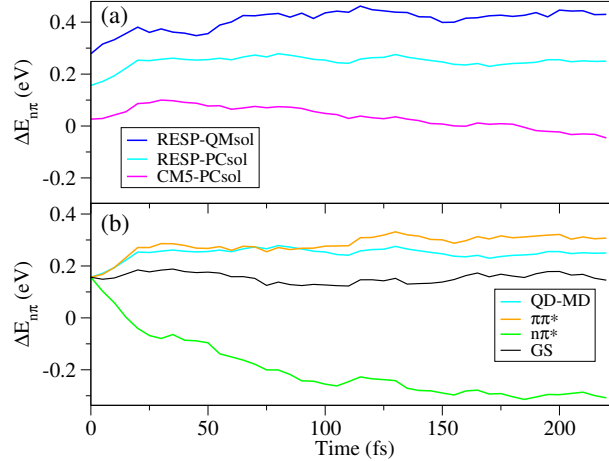


Figure 6: (a) Energy gap between $\pi\pi^*$ and $n\pi^*$ states along the three dynamics considered in Figure 5: RESP/QMsol, CM5/QMsol and CM5/PCsol models. In panel (b) we focus on the RESP/PCsol and for comparison we report the extreme cases in which the solute is frozen in $\pi\pi^*$, $n\pi^*$ or GS.

The molecular models used to represent the solvent allow us to correlate the solvent dynamical effects on $\Delta E_{n\pi}^0$, i.e. on the solute nonadiabatic QD, with some key structural movement of the first solvation shell. To that end we computed the radial distribution function (RDF) of H-bonds around the two oxygen atoms of Thy as a function of time. The main scope of the present analysis is to obtain an estimation of the time scale of the solvent response. Therefore we found more convenient to focus here on the case where the system is frozen in $\pi\pi^*$ state ($P_\pi=1$) after the excitation. By doing so, we avoid the noise induced by the nonadiabatic dynamics (affected in turn by the static and dynamic solvent effect). Moreover, since the calculations are faster, this choice also allow us to have better statistics, running up to 300 trajectories. Figure 7 shows that on the 50 fs time scale the

H-bonds are already modified: the H-bond at the Oxygen 7 (whose charge density decreases in the $\pi\pi^*$ state, see Figure 1) elongates while the one at Oxygen 8 (its charge density increases) becomes shorter. Further analysis in the SI shows that for an excitation on $n\pi^*$ the evolution of the RDF is remarkably different and an hydrogen bond with O₈ is progressively lost. For what concerns the coupled QD-MD dynamics, the RDF is expected to change from case to case. In SI we show that for RESP/PCsol, where the transfer to $n\pi^*$ is quite limited but not negligible (~ 0.2 at 200 fs), the RDF is similar to what seen for a solute in $\pi\pi^*$ state, especially at short times, while at long time some features compatible with the population of $n\pi^*$ arise.

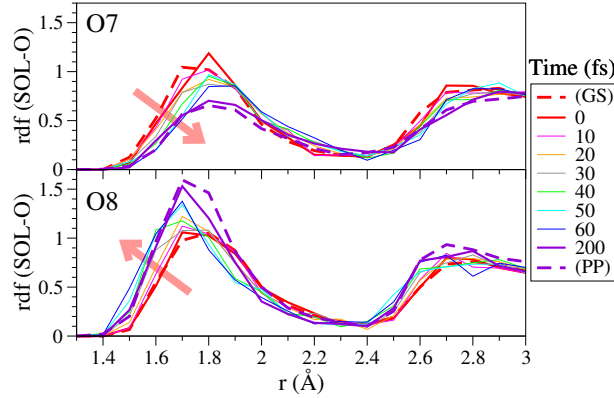


Figure 7: Radial distribution function (rdf) between the solvent (SOL) and oxygen atoms over thymine (O7 and O8) computed at different times after excitation to the $\pi\pi^*$ state (characterized by the RESP charges computed for this state). Averages over 300 trajectories. The trend of the plots with time is indicated with pale red arrows. The curves (GS) and (PP) correspond to an average with 1000 points taken from a simulation of 10 ns on GS and $\pi\pi^*$ state, respectively, after 200 ps of equilibration.

5 Discussion

5.1 Physical insight into the dynamical solvent effect

The calculations reported above clearly indicate that the population transfer is significantly reduced when going from gas phase to water. The amount of $n\pi^*$ population drastically depends on the computed $\Delta E_{n\pi}^0$ and, therefore, on the adopted solvation model. For example, after ~ 100 fs, the time associated to direct decay of $\pi\pi^*$ to GS,^{19,23} CM5/PCsol predicts a population on $n\pi^*$ 15-20 times larger than RESP/QMsol (Figure 5). A cluster model often adopted in the literature,²² comprising Thy and 4 explicit solvent molecules embedded in PCM, provides for $\Delta E_{n\pi}^0$ a value of 0.25~0.3 eV (PBE0/6-31+G(d,p)). Both RESP/QMsol and RESP/PCsol provide $\Delta E_{n\pi}^0$ values consistent with this reference value. Our 'best' QD-MD calculations thus predict that after ~ 100 fs only a minor part, between $\sim 2\%$ and $\sim 10\%$, of the photoexcited population is on $n\pi^*$. RI-CC2⁴⁴ and MS-CASPT2/ANO-L (on Uracil)⁴⁸ predict even larger energy gaps in solution so that the $n\pi^*$ population would be vanishingly small. From the experimental point of view, Hare et al.¹⁸ estimated a transfer to $n\pi^*$ by $\sim 10\%$ while, more recently, Buchner et al.¹⁹ did not observe signatures of a population of $n\pi^*$.

On more general grounds, our study provides significant insights on solvent effects on IC, allowing to discriminate the relative importance of different factors like: (i) the modification of the average relative position and shape of the coupled PES (average static effects), (ii) the fact that solute molecules in different solvent cavities experience different energy gaps (static disorder) and, finally, (iii) the true dynamical response to the solute nonadiabatic dynamics.

The huge difference between the population transfer predicted in gas phase

and in water, observed with Av ΔE model, independently of the adopted solvation model, suffices to illustrate the importance of the first point. Static disorder plays a remarkable role. Fluct ΔE results show that even assuming that the solvent is too slow to respond on the IC timescale -as it should be the case for slow aprotic solvents- the existence of different solvent configurations on GS has an effect on the IC that can be completely overlooked by a single dynamics on averaged PES. This is predicted to be especially true when the population transfer falls in one of the two opposite regimes: very small or very large. For example, at 230 fs using RESP/QMsol P_n is 0.015 according to Av ΔE and 0.1 for Fluct ΔE , an increase by a factor 6-7 (Figure 3).

More importantly, our results highlight that water true dynamical response has an impact on the IC yield even on the femtosecond time scale ~ 50 fs, and is mediated by its librational motions that modify the H-bond pattern. The same time scale was measured very recently by broad band pump-probe spectroscopy for the ultrafast water dynamics around a photoexcited rhodamine or a photoexcited protein, and attributed to librational motions.⁴⁹ Inspection of Figure 5 shows that not only the 'final' amount of P_n population is noticeably affected by solvent dynamics, but that also the trends can be different. For example, for RESP/QMsol case, when solvent dynamics is not accounted for, P_π decreases progressively up to 230 fs. On the contrary, according to QD-MD, after a transient ultrafast decrease for $t < 50$ fs, P_π starts increasing again as a result of the solvent stabilization of the $\pi\pi^*$ state. In this case solvent dynamical effect quenches the population transfer restoring a behaviour more similar to what predicted by simple Av ΔE model. In other cases however, like for RESP/CM5sol, the decay remains similar to the Fluct ΔE case, or it is even enhanced by solvent dynamics at long times when, due to the progressive population of $n\pi^*$, $\Delta E_{n\pi}^0$ start decreasing with time.

These differences are significant in themselves, and they could become even more important, when considering all the other possible excited state decay paths of Thy, or systems with a larger number of coupled excited states.

Finally we also showed that it is very important to account for polarizability of the first shell of water molecules. In fact QMsol predictions for $n\pi^*$ population are significantly smaller than PCsol ones. Figure 3 shows that even without accounting for solvent dynamical effects, the long-time limit of P_n with Fluct ΔE /CM5 model increases drastically from ~ 0.1 (QMsol) to ~ 0.5 (PCsol). The same phenomenon is observed in coupled QD-MD dynamics (compare RESP/QMsol and RESP/PCsol in Figure 5). This is a consequence of the different behavior of $\Delta E_{n\pi}^0$ (at $t=230$ fs is ~ 0.25 eV for PCsol and ~ 0.43 eV for QMsol, Figure 6). This result clearly shows the limitation of a non-polarizable description of the solvent, especially in the case of electronic transitions not involving large displacements of the electronic density, as it often happens for bright $\pi\pi^*$ transitions.

5.2 Limitations of the model and perspectives

The core ingredients of the approach we presented here are: (i) a QD treatment of the solute; (ii) a MD description of the dynamical response of an atomistic model of the solvent, and (iii) a mean-field approximation to derive the coupling of the quantum and classical systems.

For what concerns QD calculations, the adoption of a simple (LVC or QVC) model potential for the solute PES is not a fundamental requisite of the method, since, as we commented in Section II, this might be considered simply as a “local expansion” of the potentials around the position where the wavepacket is localized. In this sense our approach might be seen as a possible route to include dynamical solvent effects in on-the-fly QD propagations, like those performed with DD-vMCG

method.^{27,28} However, at the state of the art, QD-MD simulation on-the-fly of a nonadiabatic process in solution would require a formidable effort. Therefore our approach is currently limited to rigid systems amenable for a description of the PES with a truncated (e.g. quadratic) Taylor expansion. Classical methods like Trajectory Surface Hopping (TSH) on the contrary are very effective and, by construction, perfectly suitable to run on-the-fly simulations, and they can introduce the dynamical solvent effect without the mean-field approximation we invoked. On the other side they provide an approximate description of the nonadiabatic transition of the system wavepacket.⁵⁰

Beyond the above mentioned core characteristics of our method, in this first application we made a number of technical choices and approximations that are not intrinsic in the method and can be in principle modified, although additional and tailored studies are necessary to inquire their effect on the dynamics and to optimize the computational cost.

In this contribution all the feedback of the solvent dynamics is concentrated on the energy gap $\Delta E_{n\pi}^0$. Although we have shown that this is indeed the dominant parameter to study the solvent dynamical effect on the $\pi\pi^*/n\pi^*$ internal conversion in Thy, other parameters of the Hamiltonian can be allowed to change with time. For example, the constant term in the coupling in Eq. 7 could depend on the instantaneous position of the solvent. This would account for the possibility that the solvent cavity lifts the degeneracy of the diabatic surfaces.

The parameters of the Hamiltonian kept constant during the simulation were obtained with PCM, i.e. within a mean-field approximation, and considered equal for each solvent snapshot. It would be instead possible, to recompute different values for these parameters for each solvent snapshot. This is the proper framework to include not only the solvent lifting of the CoI, but also the effect of the dynamical

polarization of the solute due to the solvent dynamics. This approach would, however remarkably increase the computational cost of the protocol; moreover notice that, if all the parameters of the Hamiltonian are made time-dependent and re-computed during the dynamics, we fall in the general case of the on-the-fly quantum dynamics described above, which cannot be routinely used for molecules in solution.

As far as the solvent is concerned, in the calculations here reported its motion was driven by a standard MM Force Field. However, more sophisticated schemes could be introduced for the interaction with the solute, allowing the solvent to interact directly with the electronic densities of the solute. This might be done replacing in the Coulomb potential the atomic charges of the two states with a discrete (cube) representation of their corresponding QM electronic densities. The differences obtained by using RESP or CM5 charges suggest that such an improved scheme is actually needed to obtain more accurate results.

At the same time, it is in principle possible to adopt a polarizable force field for the solvent, so to investigate the mutual polarization of the solute and solvent and how it changes during the dynamics. For the time being we notice that, despite recent remarkable developments on QM/MM schemes for MD, also accounting for polarizable MM potentials,^{51,52} their adoption is not even standard in ground state MD runs for the computation of electronic spectra (in fact often a standard MM force field is preferred to run in reasonable time the long simulations necessary for a reliable sampling).^{32,33,53-58} On the same foot, even in fully classical TSH calculations of nonadiabatic processes non-polarizable force fields are a popular choice, both in solution^{23,59,60} and in supramolecular environments.^{61,62} Therefore the implementation of these improvements in our QD-MD coupled method require extensive testing and well planned studies and will be the object of future studies.

We close this section noting that, in future works, it will be interesting to analyse in depth the performance of our QD-MD method with respect to the characteristics of different solvents like polarity and proticity, and to design suitable simple model systems where reference full QD calculations are possible so to extensively investigate the accuracy of the mean-field approximation with respect to the velocity and magnitude of the solvent response and to the typical frequency of the most involved solvent modes. If necessary, some high-frequency solute-solvent modes might be included in the set of modes to be treated with quantum dynamics.

6 Conclusions

In this contribution we presented a simple mixed quantum/classical method to investigate the dynamics of an internal conversion in solution, describing the solute with quantum dynamics and accounting for the dynamical response of an atomistic solvent model in classical approximation. The coupling of solute and solvent dynamics is obtained with a mean-field scheme. The method was applied to the $\pi\pi^* \rightarrow n\pi^*$ population transfer of Thymine in water showing remarkable dynamical solvent effects on the internal conversion dynamics.

In the realm of methods that preserve a QD treatment for some of the nuclear DoFs, several recently-proposed QD or MQC propagations schemes are potentially applicable to solute/solvent dynamics and here it is not possible to review them.^{15,25,26,63–69} The specificity of our QD-MD method is that it retains a full QD description of the solute DoF and a molecular model for the solvent. Although it is based on a simplified description of the solvent effects on electronic populations and coherences, it has the advantage to be very effective and computationally cheap. This has made possible to get new physical insights on solvent effect by ex-

ploring the predictions of several different solvent models with a sufficient number of trajectories to get statistically stable results.

Beyond its effectiveness, our approximated method, by using model Hamiltonians and treating on different foot the solute and the solvent degrees of freedom, implements a model of the dynamics that facilitate a simple chemical picture of the results in terms of a solute process (the system) perturbed by the solvent (the environment). It also allows to focalize the analysis on the effect of few chemically intuitive parameters or descriptors. Here we considered the energy gap, but other parameters can be taken into account in future work thus obtaining a more complete model. In methods like TSH analogous analyses are of course possible, but since all coordinates are treated on the same foot, a non trivial post processing of the data may be needed to deconvolve the effect of the solute and the solvent and to individuate few descriptors of the main dynamical solvent effect.

A number of generalizations of our method have been discussed in the previous section. Additional extensions are possible. For instance, in the future we might explore the possibility to include part of the solute modes in the classical partition, thus opening the route to the application to very large systems, or floppy tuning modes. Even considering the method in its present implementation, it is expected that the straightforward definition of the system Hamiltonian reported here, together with the high computational efficiency, will make it suitable for further applications to photophysical processes in complex scenarios, like in the case of energy and charge transfers in multichromophoric systems in solution, where quantum vibrational effects are very important. Finally, we think that comparisons of the predictions of this QD-MD method and semiclassical approaches like TSH on well designed model systems may reveal useful to analyse if decoherence and dissipative effects due to the solvent hampers and to what extent the difference

between quantum and classical predictions.

Acknowledgement

The support of MIUR (PRIN 2010-2011 prot. 2010ERFKXL) is acknowledged. J.C. acknowledges the Fundación Ramón Areces for funding his Postdoctoral position in Pisa and the fellowship provided by “Fundación Séneca – Agencia de Ciencia y Tecnología de la Región de Murcia” through the “Saavedra-Fajardo” program (20028/SF/16). R.I. thanks the Université Paris-Saclay (Chaire d’Alembert No. 2016-10751). Y. L. acknowledges the financial support from the China Scholarship Council (CSC, No. 201506220064) and Y.L. and N. L. a generous grant of computer time from the Norwegian Programme for Supercomputing. N. L. also acknowledges the National Nature Science Foundation of China (Grant No. 21573129). The authors gratefully acknowledge G. Worth for making available the Quantics code and for useful discussions.

Supporting Information Available

RESP and CM5 solvent charges. Convergence checks of the QD and QD-MD. Tests for choosing Δt and number of trajectories for the averages. RDF computed for dynamics on GS and on $n\pi^*$ states and for a coupled QD-MD simulation.

References

- (1) Domcke, W., Yarkony, R., Köppel, H., Eds. *Conical Intersections, Electronic Structure, Dynamics and Spectroscopy*; World Scientific Publishing Co. Singapore, 2004.
- (2) Beck, M. H.; Jäckle, A.; Worth, G. A.; Meyer, H.-D. The multiconfiguration time-dependent Hartree method: A highly efficient algorithm for propagating wavepackets. *Phys. Rep.* **2000**, *324*, 1–105.
- (3) Wang, H.; Thoss, M. Multilayer formulation of the multiconfiguration time-dependent Hartree theory. *J. Chem. Phys.* **2003**, *119*, 1289–1299.
- (4) Wang, H.; Thoss, M. Multilayer formulation of the multiconfiguration time-dependent Hartree theory. *J. Chem. Phys.* **2003**, *119*, 1289–1299.
- (5) Manthe, U. A multilayer multiconfigurational time-dependent Hartree approach for quantum dynamics on general potential energy surfaces. *J. Chem. Phys.* **2008**, *128*, 164116.
- (6) Manthe, U. Layered discrete variable representations and their application within the multiconfigurational time-dependent Hartree approach. *J. Chem. Phys.* **2009**, *130*, 054109.
- (7) Vendrell, O.; Meyer, H.-D. Multilayer multiconfiguration time-dependent Hartree method: Implementation and applications to a Henon-Heiles Hamiltonian and to pyrazine. *J. Chem. Phys.* **2011**, *134*, 044135.
- (8) Hughes, K. H.; Christ, C. D.; Burghardt, I. Effective-mode representation of non-Markovian dynamics: A hierarchical approximation of the spectral

- density. I. Application to single surface dynamics. *J. Chem. Phys.* **2009**, *131*, 024109.
- (9) Hughes, K. H.; Christ, C. D.; Burghardt, I. Effective-mode representation of non-Markovian dynamics: A hierarchical approximation of the spectral density. II. Application to environment-induced nonadiabatic dynamics. *J. Chem. Phys.* **2009**, *131*, 124108.
- (10) Burghardt, I.; Martinazzo, R.; Hughes, K. H. Non-Markovian reduced dynamics based upon a hierarchical effective-mode representation. *J. Chem. Phys.* **2012**, *137*, 144107.
- (11) Non-Markovian reduced dynamics of ultrafast charge transfer at an oligothiophene-fullerene heterojunction. *Chem. Phys.* **2014**, *442*, 111–118.
- (12) Liu, H.; Zhu, L.; Bai, S.; Shi, Q. Reduced quantum dynamics with arbitrary bath spectral densities: Hierarchical equations of motion based on several different bath decomposition schemes. *J. Chem. Phys.* **2014**, *140*, 134106.
- (13) De carvahlo, F. F.; Bouduban, M. E. F.; Curchod, B. F. E.; Tavernelli, I. Nonadiabatic molecular dynamics based on trajectories. *Entropy* **2014**, *16*, 62–85.
- (14) Barbatti, M.; Ruckebauer, M.; Plasser, F.; Pittner, J.; Granucci, G.; Persico, M.; Lischka, H. Newton-X: a surface-hopping program for nonadiabatic molecular dynamics. *WIREs Comput. Mol. Sci.* **2014**, *4*, 26–33.
- (15) Curchod, B. F. E.; Rauer, C.; Marquetand, P.; González, L.; Martínez, T. J. Communication: GAIMS-Generalized Ab Initio Multiple Spawning for both internal conversion and intersystem crossing processes. *J. Chem. Phys.* **2016**, *144*, 101102.

- (16) Improta, R.; Barone, V.; Lami, A.; Santoro, F. Quantum Dynamics of the Ultrafast $\pi\pi^* \rightarrow n\pi^*$ Population Transfer in Uracil and 5-Fluoro-Uracil in Water and Acetonitrile. *J. Phys. Chem. B* **2009**, *113*, 14491–14503.
- (17) Thallmair, S.; Zauleck, J. P. P.; de Vivie-Riedle, R. Quantum Dynamics in an Explicit Solvent Environment: A Photochemical Bond Cleavage Treated with a Combined QD/MD Approach. *J. Chem. Theory Comput.* **2015**, *11*, 1987–1995, PMID: 26574404.
- (18) Hare, P. M.; Crespo-Hernández, C. E.; Kohler, B. Internal conversion to the electronic ground state occurs via two distinct pathways for pyrimidine bases in aqueous solution. *Proc. Natl. Acad. Sci.* **2007**, *104*, 435–440.
- (19) Buchner, F.; Nakayama, A.; Yamazaki, S.; Ritze, H.-H.; Lübcke, A. Excited-State Relaxation of Hydrated Thymine and Thymidine Measured by Liquid-Jet Photoelectron Spectroscopy: Experiment and Simulation. *J. Am. Chem. Soc.* **2015**, *137*, 2931–2938.
- (20) Xue, B.; Yabushita, A.; Kobayashi, T. Ultrafast dynamics of uracil and thymine studied using a sub-10 fs deep ultraviolet laser. *Phys. Chem. Chem. Phys.* **2016**, *18*, 17044–17053.
- (21) Prokhorenko, V. I.; Picchiotti, A.; Pola, M.; Dijkstra, A. G.; Miller, R. J. D. New Insights into the Photophysics of DNA Nucleobases. *J. Phys. Chem. Lett.* **2016**, *7*, 4445–4450.
- (22) Improta, R.; Santoro, F.; Blancafort, L. Quantum mechanical studies on the Photophysics and the Photochemistry of nucleic acids and nucleobases. *Chem. Rev.* **2016**, *116*, 3540–3593.

- (23) Nakayama, A.; Arai, G.; Yamazaki, S.; Taketsugu, T. Solvent effects on the ultrafast nonradiative deactivation mechanisms of thymine in aqueous solution: Excited-state QM/MM molecular dynamics simulations. *J. Chem. Phys.* **2013**, *139*, 214304.
- (24) Köppel, H.; Domcke, W.; Cederbaum, L. The Multi-mode vibronic-coupling approach . Conical Intersections, Electronic Structure, Dynamics and Spectroscopy. 2004; pp 323–368.
- (25) Burghardt, I.; Nest, M.; Worth, G. A. Multiconfigurational system-bath dynamics using Gaussian wave packets: Energy relaxation and decoherence induced by a finite-dimensional bath. *J. Chem. Phys.* **2003**, *119*, 5364–5378.
- (26) Burghardt, I.; Giri, K.; Worth, G. A. Multimode quantum dynamics using Gaussian wavepackets: The Gaussian-based multiconfiguration time-dependent Hartree (G-MCTDH) method applied to the absorption spectrum of pyrazine. *J. Chem. Phys.* **2008**, *129*, 174104.
- (27) Lasorne, B.; Robb, M. A.; Worth, G. A. Direct quantum dynamics using variational multi-configuration Gaussian wavepackets. Implementation details and test case. *Phys. Chem. Chem. Phys.* **2007**, *9*, 3210–3227.
- (28) Asturiol, D.; Lasorne, B.; Worth, G. a.; Robb, M. a.; Blancafort, L. Exploring the sloped-to-peaked S2/S1 seam of intersection of thymine with electronic structure and direct quantum dynamics calculations. *Phys. Chem. Chem. Phys.* **2010**, *12*, 4949–4958.
- (29) Polyak, I.; Allan, C. S. M.; Worth, G. A. A complete description of tunnelling using direct quantum dynamics simulation: Salicylaldehyde proton transfer. *J. Chem. Phys.* **2015**, *143*, 084121.

- (30) Multi-state non-adiabatic direct-dynamics on propagated diabatic potential energy surfaces. *Chem. Phys. Lett.* **2017**, *683*, 606–612.
- (31) Tomasi, J.; Mennucci, B.; Cammi, R. Quantum Mechanical Continuum Solvation Models. *Chem. Rev.* **2005**, *105*, 2999–3094.
- (32) Cerezo, J.; Avila Ferrer, F. J.; Prampolini, G.; Santoro, F. Modeling solvent broadening on the vibronic spectra of a series of coumarin dyes. From implicit to explicit solvent models. *J. Chem. Theory Comput.* **2015**, *11*, 5810–5825.
- (33) Zalenśy, R.; Murugan, N. A.; Gelmukhanov, F.; Rinkevicius, Z.; Ośmiałowski, B.; Bartkowiak, W.; Ågren, H. Toward Fully Nonempirical Simulations of Optical Band Shapes of Molecules in Solution: a Case Study of Heterocyclic Ketoimine Difluoroborates. *J. Phys. Chem. A* **2015**, *119*, 5145–5152.
- (34) Frisch, M. J. et al. Gaussian 09 Revision D.1. 2009; Gaussian Inc. Wallingford CT.
- (35) Cimiraglia, R.; Malrieu, J.-P.; Maurizio, P.; Fernand, S. Quasi-diabatic states and dynamical couplings from ab initio CI calculations: a new proposal. *J. Phys. B: At. Mol. Phys.* **1985**, *18*, 3073–3084.
- (36) Neugebauer, J.; Baerends, E. J.; Nooijen, M. Vibronic coupling and double excitations in linear response time-dependent density functional calculations: Dipole-allowed states of N₂. *J. Chem. Phys.* **2004**, *121*, 6155–6166.
- (37) Isborn, C. M.; Mar, B. D.; Curchod, B. F. E.; Tavernelli, I.; Martínez, T. J. The Charge Transfer Problem in Density Functional Theory Calculations of Aqueously Solvated Molecules. *J. Phys. Chem. B* **2013**, *117*, 12189–12201, PMID: 23964865.

- (38) Worth, G. A.; Giri, K.; Richings, G. W.; Beck, M. H.; Jäckle, A.; Meyer, H.-D. The QUANTICS Package, Version 1.1, (2015), University of Birmingham, Birmingham, U.K.
- (39) Wang, J.; Cieplak, P.; Kollman, P. A. How well does a restrained electrostatic potential (RESP) model perform in calculating conformational energies of organic and biological molecules? *J. Comput. Chem.* **2000**, *21*, 1049–1074.
- (40) Marenich, A. V.; Jerome, S. V.; Cramer, C. J.; Truhlar, D. G. Charge Model 5: An Extension of Hirshfeld Population Analysis for the Accurate Description of Molecular Interactions in Gaseous and Condensed Phases. *J. Chem. Theory Comput.* **2012**, *8*, 527–541.
- (41) Improta, R.; Scalmani, G.; Frisch, M. J.; Barone, V. Toward effective and reliable fluorescence energies in solution by a new state specific polarizable continuum model time dependent density functional theory approach. *J. Chem. Phys.* **2007**, *127*, 074504.
- (42) Szalay, P. G.; Watson, T.; Perera, A.; Lotrich, V. F.; Bartlett, R. J. Benchmark Studies on the Building Blocks of DNA. 1. Superiority of Coupled Cluster Methods in Describing the Excited States of Nucleobases in the Franck-Condon Region. *J. Phys. Chem. A* **2012**, *116*, 6702–6710, PMID: 22587574.
- (43) Picconi, D.; Barone, V.; Lami, A.; Santoro, F.; Improta, R. The Interplay between $\pi\pi^*/n\pi^*$ Excited States in Gas-Phase Thymine: A Quantum Dynamical Study. *ChemPhysChem* **2011**, *12*, 1957–1968.
- (44) Etinski, M.; Marian, C. M. Ab initio investigation of the methylation and hydration effects on the electronic spectra of uracil and thymine. *Phys. Chem. Chem. Phys.* **2010**, *12*, 4915–4923.

- (45) Wolf, T. et al. Probing ultrafast $\pi\pi^*/n\pi^*$ internal conversion in organic chromophores via K-edge resonant absorption. *Nat. Commun.* **2017**, *8*, 29.
- (46) Keutsch, F. N.; Fellers, R. S.; Brown, M. G.; Viant, M. R.; Petersen, P. B.; Saykally, R. J. Hydrogen Bond Breaking Dynamics of the Water Trimer in the Translational and Librational Band Region of Liquid Water. *J. Am. Chem. Soc* **2001**, *123*, 5938–5941.
- (47) Petersen, J.; Møller, K. B.; Rey, R.; Hynes, J. T. Ultrafast Librational Relaxation of H₂O in Liquid Water. *J. Phys. Chem. B* **2013**, *117*, 4541–4552.
- (48) Bistafa, C.; Georg, H. C.; Canuto, S. Combining ab initio multiconfigurational and Free Energy Gradient methods to study the $\pi\pi^*$ excited state structure and properties of uracil in water. *Comput. Theoret. Chem.* **2014**, *1040–1041*, 312–320.
- (49) Jumper, C. C.; Arpin, P. C.; Turner, D. B.; McClure, S. D.; Rafiq, S.; Dean, J. C.; Cina, J. A.; Kovac, P. A.; Mirkovic, T.; Scholes, G. D. Broad-Band Pump-Probe Spectroscopy Quantifies Ultrafast Solvation Dynamics of Proteins and Molecules. *J. Phys. Chem. Lett.* **2016**, *7*, 4722–4731.
- (50) Tully, J. C. Molecular dynamics with electronic transitions. *J. Chem. Phys.* **1990**, *93*, 1061–1071.
- (51) Lipparini, F.; Lagardère, L.; Raynaud, C.; Stamm, B.; Cancès, E.; Mennucci, B.; Schnieders, M.; Ren, P.; Maday, Y.; Piquemal, J.-P. Polarizable Molecular Dynamics in a Polarizable Continuum Solvent. *J. Chem. Theory Comput.* **2015**, *11*, 623–634.
- (52) Loco, D.; Lagardère, L.; Caprasecca, S.; Lipparini, F.; Mennucci, B.; Piquemal, J.-P. Hybrid QM/MM Molecular Dynamics with AMOEBA Polariz-

- able Embedding. *J. Chem. Theory Comput.* **2017**, *13*, 4025–4033, PMID: 28759205.
- (53) Sjoqvist, J.; Linares, M.; Lindgren, M.; Norman, P. Molecular dynamics effects on luminescence properties of oligothiophene derivatives: a molecular mechanics-response theory study based on the CHARMM force field and density functional theory. *Phys. Chem. Chem. Phys.* **2011**, *13*, 17532–17542.
- (54) De Mitri, N.; Monti, S.; Prampolini, G.; Barone, V. Absorption and Emission Spectra of a Flexible Dye in Solution: A Computational Time-Dependent Approach. *J. Chem. Theory Comput.* **2013**, *9*, 4507–4516.
- (55) Cacelli, I.; Ferretti, A.; Prampolini, G. Perturbative Multireference Configuration Interaction (CI-MRPT2) Calculations in a Focused Dynamical Approach: A Computational Study of Solvatochromism in Pyrimidine. *J. Phys. Chem. A* **2015**, *119*, 5250–5259, PMID: 25386718.
- (56) Del Frate, G.; Bellina, F.; Mancini, G.; Marianetti, G.; Minei, P.; Pucci, A.; Barone, V. Tuning of dye optical properties by environmental effects: a QM/MM and experimental study. *Phys. Chem. Chem. Phys.* **2016**, *18*, 9724–9733.
- (57) Zuehlsdorff, T. J.; Haynes, P. D.; Hanke, F.; Payne, M. C.; Hine, N. D. M. Solvent Effects on Electronic Excitations of an Organic Chromophore. *J. Chem. Theory Comput.* **2016**, *12*, 1853–1861, PMID: 26967019.
- (58) Loco, D.; Jurinovich, S.; Bari, L. D.; Mennucci, B. A fast but accurate excitonic simulation of the electronic circular dichroism of nucleic acids: how can it be achieved? *Phys. Chem. Chem. Phys.* **2016**, *18*, 866–877.

- (59) Ruckenbauer, M.; Barbatti, M.; Müller, T.; Lischka, H. Nonadiabatic Photo-dynamics of a Retinal Model in Polar and Nonpolar Environment. *J. Phys. Chem. A* **2013**, *117*, 2790–2799.
- (60) Cantatore, V.; Granucci, G.; Persico, M. Simulation of the $\pi \rightarrow \pi^*$ photo-dynamics of azobenzene: Decoherence and solvent effects. *Comput. Theoret. Chem.* **2014**, *1040*, 126–135, Excited states: From isolated molecules to complex environments.
- (61) Cantatore, V.; Granucci, G.; Rousseau, G.; Padula, G.; Persico, M. Photoisomerization of Self-Assembled Monolayers of Azobiphenyls: Simulations Highlight the Role of Packing and Defects. *J. Phys. Chem. Lett.* **2016**, *7*, 4027–4031.
- (62) Conti, I.; Nenov, A.; Hofinger, S.; Flavio Altavilla, S.; Rivalta, I.; Dumont, E.; Orlandi, G.; Garavelli, M. Excited state evolution of DNA stacked adenines resolved at the CASPT2//CASSCF/Amber level: from the bright to the excimer state and back. *Phys. Chem. Chem. Phys.* **2015**, *17*, 7291–7302.
- (63) Huo, P.; Bonella, S.; Chen, L.; Coker, D. Linearized approximations for condensed phase non-adiabatic dynamics: Multi-layered baths and Brownian dynamics implementation. *Chem. Phys.* **2010**, *370*, 87–97.
- (64) Meier, C.; Beswick, J. A. Quantum Dynamics of Complex Molecular Systems. Hybrid Quantum/Classical Dynamics Using Bohmian Trajectories. 2007; pp 369–390.
- (65) Bousquet, D.; Hughes, K. H.; Micha, D. A.; Burghardt, I. Extended hydro-dynamic approach to quantum-classical nonequilibrium evolution. I. Theory. *J. Chem. Phys.* **2011**, *134*, 064116.

- (66) Hughes, K. H.; Baxter, S. N.; Bousquet, D.; Ramanathan, P.; Burghardt, I. Extended hydrodynamic approach to quantum-classical nonequilibrium evolution. II. Application to nonpolar solvation. *J. Chem. Phys.* **2012**, *136*.
- (67) Wang, H.; Thoss, M.; Miller, W. H. Systematic convergence in the dynamical hybrid approach for complex systems: A numerically exact methodology. *J. Chem. Phys.* **2001**, *115*, 2979–2990.
- (68) Hsieh, C.-Y.; Kapral, R. Analysis of the forward-backward trajectory solution for the mixed quantum-classical Liouville equation. *J. Chem. Phys.* **2013**, *138*, 134110.
- (69) Lee, M. K.; Huo, P.; Coker, D. F. Semiclassical Path Integral Dynamics: Photosynthetic Energy Transfer with Realistic Environment Interactions. *Annu. Rev. Phys. Chem.* **2016**, *67*, 639–668.

TOC Graphic

